BABEŞ-BOLYAI UNIVERSITY

FACULTY OF CHEMISTRY AND CHEMICAL ENGINEERING

COMPUTATIONAL STUDY OF ARMCHAIR CARBON NANOTUBE JUNCTIONS

PhD THESIS ABSTRACT

MIKLÓS (căs. NAGY) Katalin

Scientific advisor:

Prof. Dr. Mircea V. DIUDEA

CLUJ-NAPOCA

2011

BABEŞ-BOLYAI University
Faculty of Chemistry and Chemical Engineering
Organic Chemistry Department
Arany J. street, no. 11, Cluj-Napoca, 400084
ROMANIA

Scientific advisor:

Prof. Dr. MIRCEA V. DIUDEA

Thesis committee:

President	Conf. Dr. Cornelia MAJDIK	BABEŞ-BOLYAI University, Cluj-Napoca
Reviewers	Prof. Dr. Titus BEU	BABEŞ-BOLYAI University, Cluj-Napoca
	Assoc. Prof. Dr. István László	Budapest University of Technology and Economics, Budapest, Hungary
	Assoc. Prof. Dr. Mihai MEDELEANU	POLITEHNICA University Timisoara

Public defense: July 15, 2011

Table of contents

KEYWORDS: carbon nanotube junctions, fullerenes, molecular modeling, DFT, PM6, counting polynomial, IPMS

Chapter 1. Introduction

1.3. Computational details

Starting geometries of fullerenes were obtained using the CaGe [47, 48] software package, while the geometries of the junctions were built manually or by the aid of the Nanos Studio [49] software package (used for attaching nanotubes). Full geometry optimizations with and without symmetry constraints were performed using the PM3 [50] and PM6 [51] semiempirical methods.

Fullerenes, tetrahedral and octahedral junctions were re-optimized at the DFT level of theory using the popular B3LYP [52] exchange-correlation density functional (Becke 88 exchange functional [53] and the correlation functional of Lee, Yang and Parr [54]). Although the structures were also optimized with smaller basis sets (3-21G* and 4-31G) in the present work only the single point calculation results obtained with the 6-31G(d,p) [55, 56] basis set are presented.

Y-junctions only at the semiempirical level were studied because of the size of the molecule.

Geometry optimizations performed with and without symmetry constraints and resulted in identical structures. Vibrational frequencies were calculated at the same theoretical level at which the optimization was done, to ensure that a true minima was found.

All calculations were performed using Gaussian 09 package [57].

Omega polynomials were computed using the Nano Studio package [49]. Map transformations of selected structures was performed using the CVNet program [58].

2.1. Tetrahedral graphitic junctions

2.1.2. Classes of tetrahedral fullerenes

Tetrahedral fullerenes can be classified according to the structural fragment that appears in the tetrahedral orientation (along the C_3 symmetry axis) as depicted in Figure 12. Each of these fragments contain three pentagons: in pattern A they are adjacent to each other (pentagon triple), in pattern B they share the central hexagon and are at one bond distance, while in pattern C they are connected to the central atom and they share pairwise one hexagon.

It is obvious that fullerenes of type A do not obey the isolated pentagon rule, however the smaller members of the other fullerene classes also have adjacent pentagons. Some of the fullerenes have pentagonal arrangements such that they belong to more than just one class, as is the case of fullerenes C_{44} (*T*), C_{52} (*T*) and C_{76} (T_d).

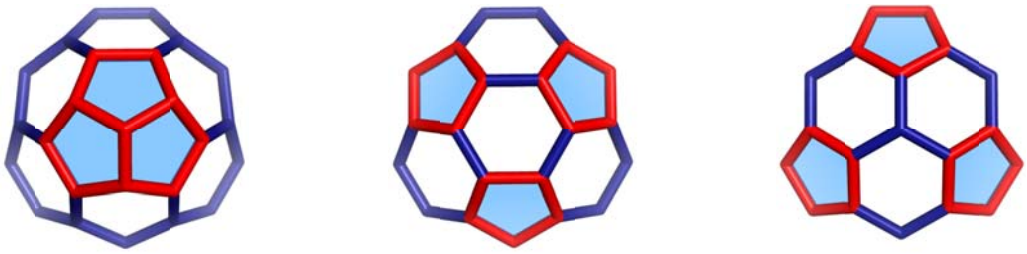

A B C

Figure 12 Structural patterns that appear in tetrahedral fullerenes. The center of each fragment is oriented along the C_3 symmetry axis.

All tetrahedral fullerenes with the number of atoms smaller than 120 were generated. While some of the fullerenes show more than one structural pattern, they were sorted according to the structural relationship to the tetrahedral junction (see below).

2.1.4. Structure of tetrahedral junctions

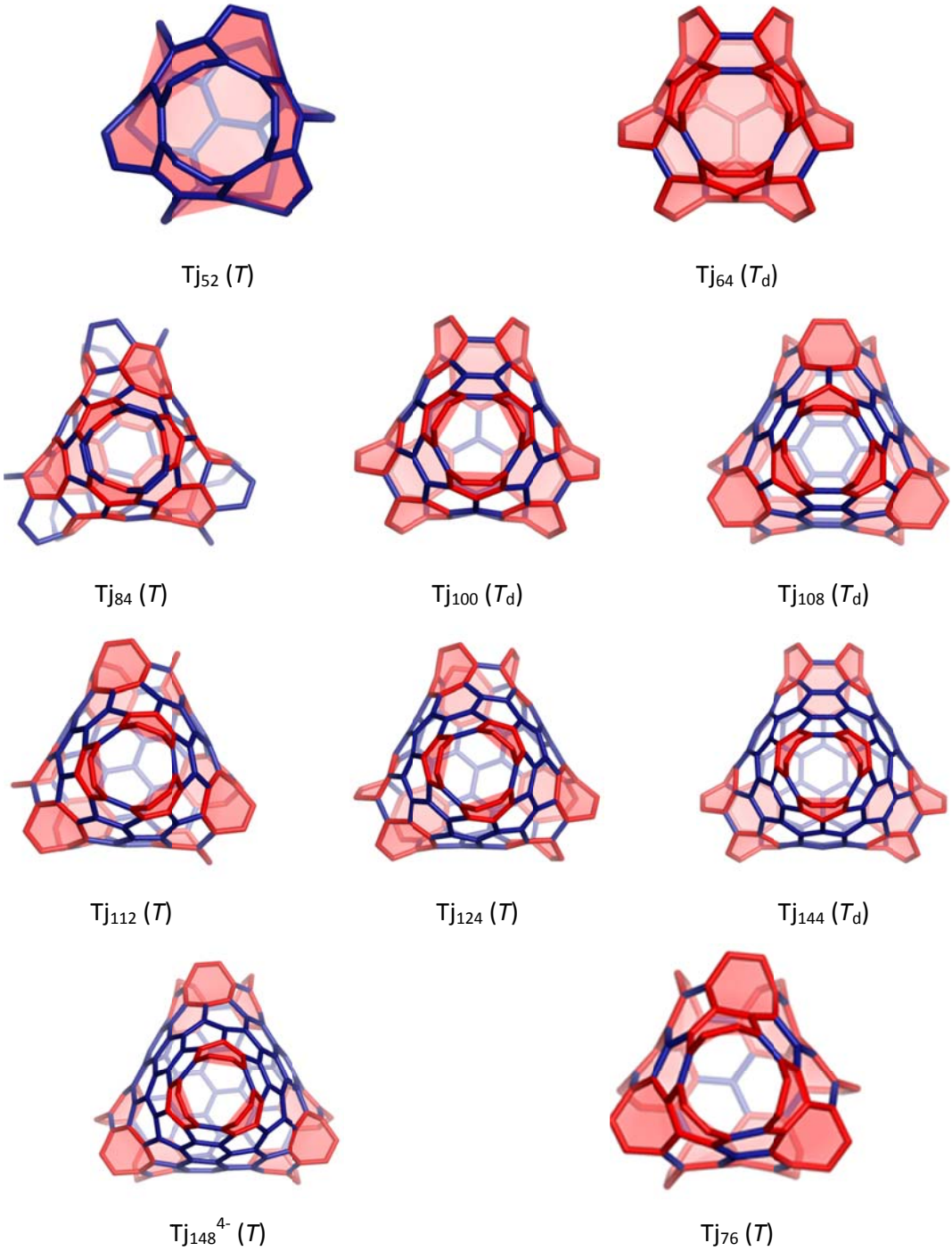

Figure 20 Tetrahedral junctions Tj(3,3) with opening chirality (3,3) viewed along the threefold axis from the top.

As it was previously presented, all possible fullerenes with tetrahedral symmetry and a number of atoms smaller than 120 were generated and classified according to the structural pattern they present. From the fullerenes belonging to class B tetrahedral junctions with armchair openings were built by homeomorph transformation of the three edges which are shared between the core hexagon and the pentagons in the structural fragment.

Attempts to build tetrahedral junctions from the other tetrahedral fullerenes (class A and C) resulted in the same structures that were obtained from the class B fullerenes. The correspondence which was found between the junctions and fullerenes is summarized in Table 3. It is obvious that the structures from a row of Table 3 can be transformed between each other by modifying (inclusion/extrusion of carbon atoms) the topology of the structural fragment.

Notice that in the last column no structure is given in the first two rows. This is because although there is a corresponding structure, it is not a classical fullerene (the number of atoms is smaller than 20). It must be mentioned that two structures have icosahedral symmetry (C_{60} and C_{80}), however they fit into the series not just by their structure but also energetically (see below).

Table 3 The correspondence between the tetrahedral junctions Tj(3,3) and the tetrahedral fullerenes from each class.

#	Tetrahedral junctions*	Tetrahedral fullerenes		
	Tj_n-TU[3,3] / f_7 = 12	C_{n-8} / pattern A	C_{n-24} / pattern B	C_{n-32} / pattern C
1	Tj_{52}^{4-} (T) / (D_2)	C_{44} (T)	C_{28}^{4-} (T_d)	–
2	Tj_{64}^{4-} (T_d) / (D_{2d})	C_{56} (T_d)	C_{40}^{4-} (T_d)	–
3	Tj_{76}^{4-} (T) / (D_2)	C_{68} (T)	C_{52}^{4-} (T)	C_{44} (T)
4	Tj_{84} (T)	C_{76}^{4-} (T)	C_{60} (I_h)	C_{52}^{4-} (T)
5	Tj_{100}^{4-} (T_d) / (D_{2d})	C_{92} (T_d)	C_{76}^{4-} (T_d)	C_{68}^{4-} (T_d)
6	Tj_{108} (T_d)	C_{100}^{4-} (T_d)	C_{84} (T_d)	C_{76}^{4-} (T_d)
7	Tj_{112}^{4-} (T) / (D_2)	C_{104} (T)	C_{88}^{4-} (T)	C_{80}^{6-} (I_h)
8	Tj_{124}^{4-} (T) / (D_2)	C_{116} (T)	C_{100}^{4-} (T)	C_{92} (T)
9	Tj_{144} (T_d)	C_{136}^{4-} (T_d)	C_{120} (T_d)	C_{112}^{4-} (T_d)
10	Tj_{148}^{4-} (T) / (D_2)	C_{140} (T)	C_{124}^{4-} (T)	C_{116} (T)

*Symmetry of the negatively charged tetrahedral junction is given first, and second the symmetry of the neutral molecule (singlet state is considered).

2.1.5. Stability of tetrahedral junctions

All structures were optimized at the B3LYP/6-31G(d,p) level of theory in singlet state. The junctions were optimized in hydrogenated form. In case of some structures charges were added as required to be able to optimize with the highest possible symmetry. Optimization of these structures in a neutral form lead to a lower symmetry structure: D_{2d} and D_2 for the structures having T_d and T topological symmetry, respectively.

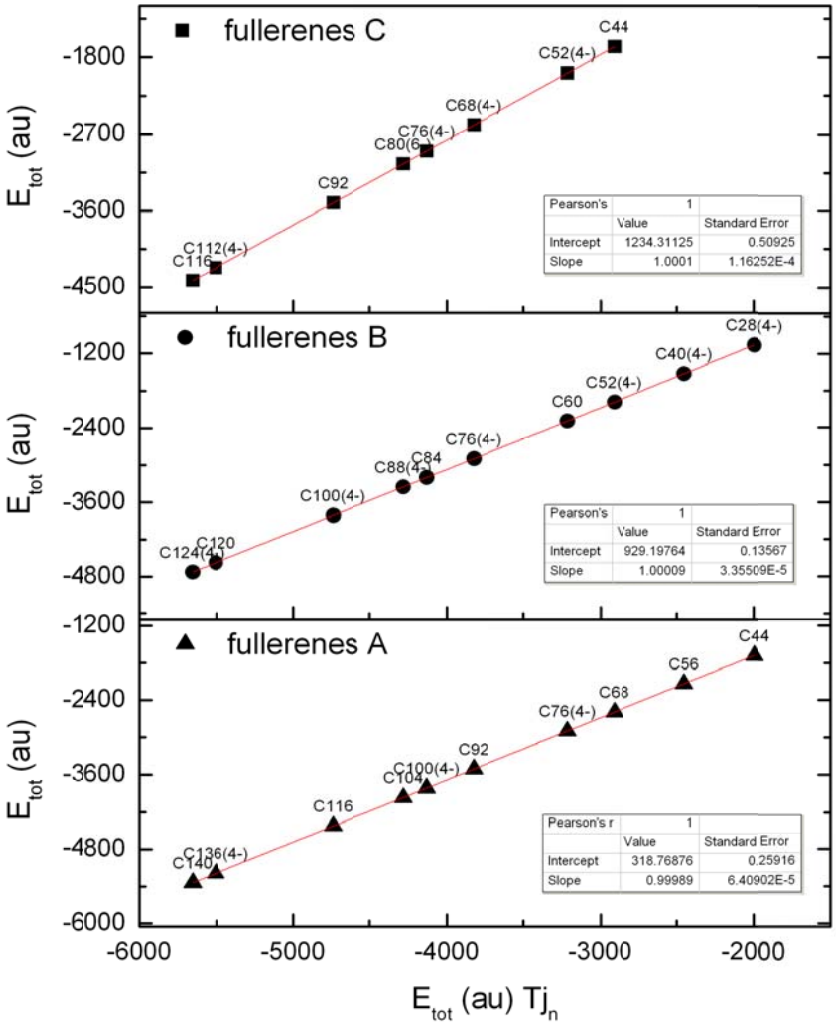

Figure 21 Plot of the total energy (a.u.) the fullerenes with structural pattern A, B and C as function of the total energy (a.u.) of the tetrahedral junctions Tj(3,3) obtained from B3LYP/6-31G(d,p) single point energy calculations.

In Figure 21 the total energy (E_{tot} in a.u.) of fullerenes from each class is plotted as function of the total energy (E_{tot} in a.u.) of the corresponding tetrahedral junction. Statistical data confirms that there is a perfect linear correlation between the total energies. This concludes that a relationship exists between the junction and the parent fullerene.

Table 4 Single point energy results (total energy E_{tot} and gap energy E_{gap}) obtained at the B3LYP/6-31G(d,p) level of theory for the neutral and negatively charged tetrahedral junctions. For a better estimation the total energy difference ΔE_{tot} is given in kcal/mol.

	E_{tot} (au)		ΔE_{tot}	E_{gap} (eV)		ΔE_{gap}
	neutral	charged (4-)	(kcal/mol)	neutral	charged (4-)	(eV)
Tj_{52} (*T*) / (D_2)	-1995.456	-1994.957	-313.249	1.433	2.167	-0.734
Tj_{64} (T_d) / (D_{2d})	-2452.628	-2452.215	-259.077	1.291	2.199	-0.908
Tj_{76} (*T*) / (D_2)	-2910.149	-2909.807	-214.850	1.260	2.330	-1.070
Tj_{100} (T_d) / (D_{2d})	-3824.692	-3824.371	-201.644	0.976	1.104	-0.128
Tj_{112} (*T*) / (D_2)	-4282.120	-4281.851	-168.892	0.905	1.091	-0.187

The stability of the neutral tetrahedral junctions with lowered symmetry (D_{2d} and D_2) and the negatively charged ones were evaluated at the B3LYP/6-31G(d,p) level of theory and are compared in Table 4. The energy difference ΔE_{tot} (presented in kcal/mol) shows that the neutral structures have a lower energy, the energy gain however decreases with the increase of the structure's size. Therefore from a thermodynamic point of view the neutral junctions show a better stability. The gap energy as a measure of kinetic stability gives a reversed order of the structures, as the last column shows in Table 4 the charged tetrahedral junctions have a larger gap. This stability difference is more pronounced in the case of the first three junctions, where ΔE_{gap} is almost one eV.

The plot in Figure 22 presents the total energy per number of carbon atoms (E_{tot}/N in au) and the gap energy (E_{gap} in au) of the tetrahedral junctions as function of the number of carbon atoms. It can be seen that the energy increases with the size of the system, although after a given size (Tj_{100}) the decrease in stability is slightly smaller.

The neutral junctions show a better kinetic stability, having a much larger energy gap than the charged structures, especially the large charged structures have a very low energy gap. However the first three charged junctions also have a relatively high gap. While there is no certain rule of stability, judging from the results it can be concluded that the first two tetrahedral junctions Tj_{52}^{4-} (*T*) and Tj_{64} (T_d) are good candidates for synthesis. Notice that the junction resulted from the C_{60} fullerene shows the best kinetic stability.

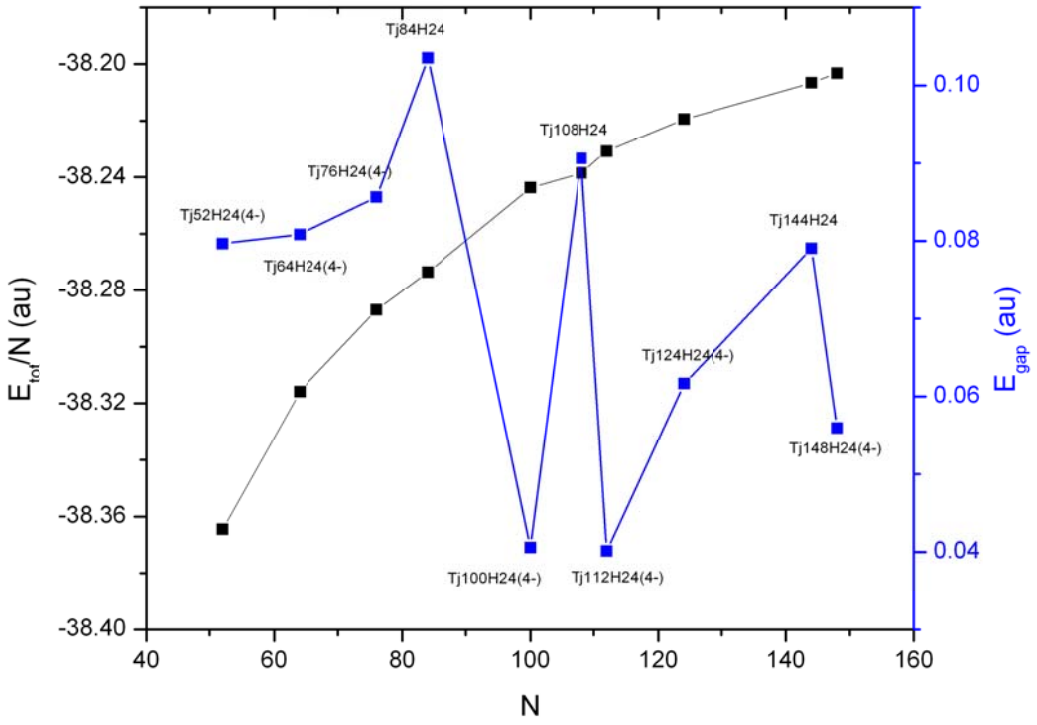

Figure 22 Plot of the tetrahedral junctions Tj(3,3) total energy per number of carbon atoms in a.u. and gap energy in a.u. as function of number of carbon atoms obtained from B3LYP/6-31G(d,p) single point energy calculations.

2.2. Octahedral graphitic junctions

2.2.2. Structure of octahedral junctions

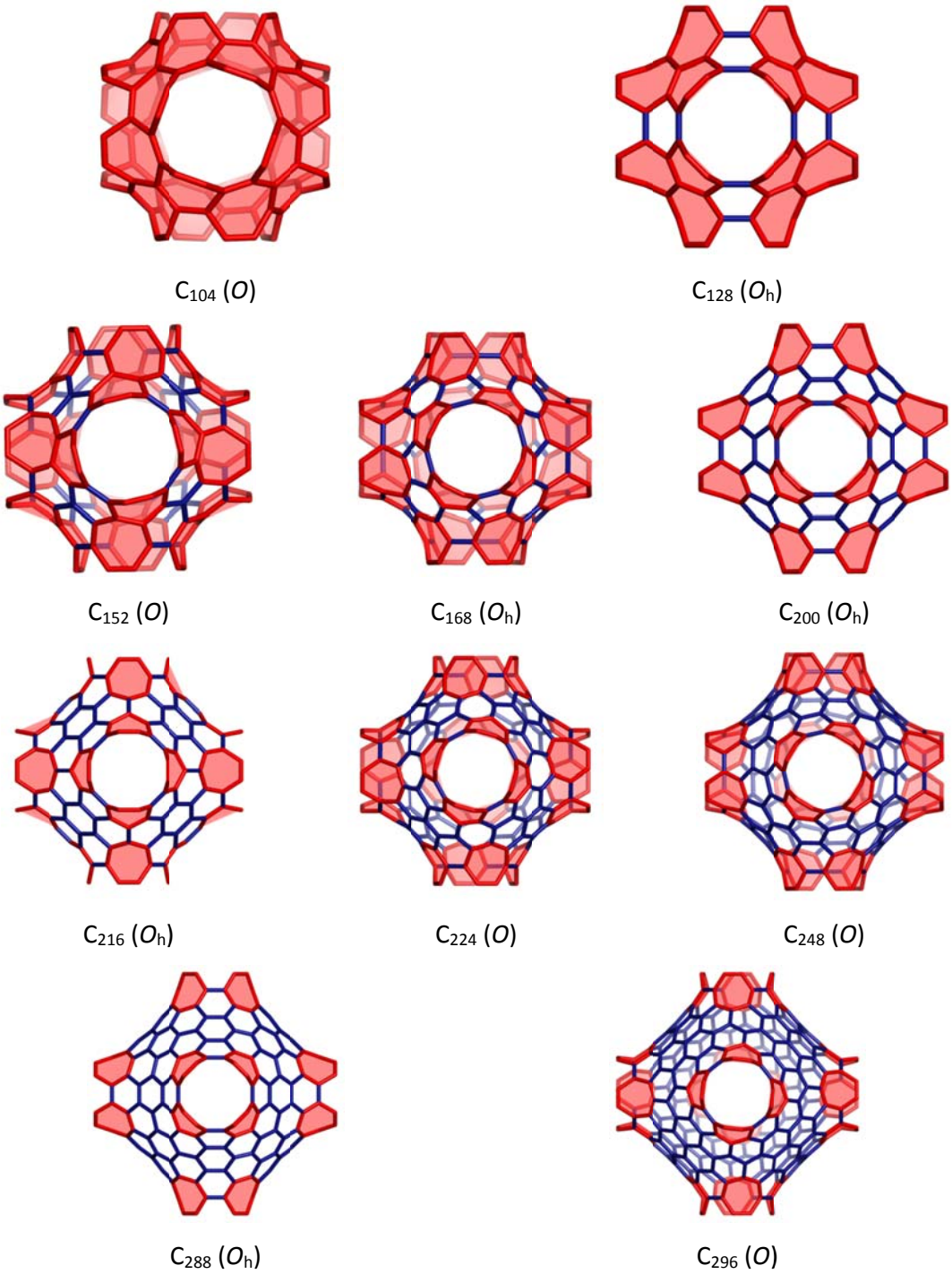

Figure 24 The octahedral junctions with (4,4) opening chirality viewed along the fourfold axis.

2.2.3. Stability of octahedral junctions

The plot in Figure 25 presents the variation of the total energy per carbon atom of the octahedral junctions as a function of the number of carbon atoms. A similar trend exists in the variation of the total energy as previously observed in the case of tetrahedral junctions, the energy rises with the size of the system. The gap energy however presents a different stability ordering. The neutral junctions have the highest gap energy. In contrast to the case of tetrahedral junctions, the smallest members of these structures have a low kinetic stability.

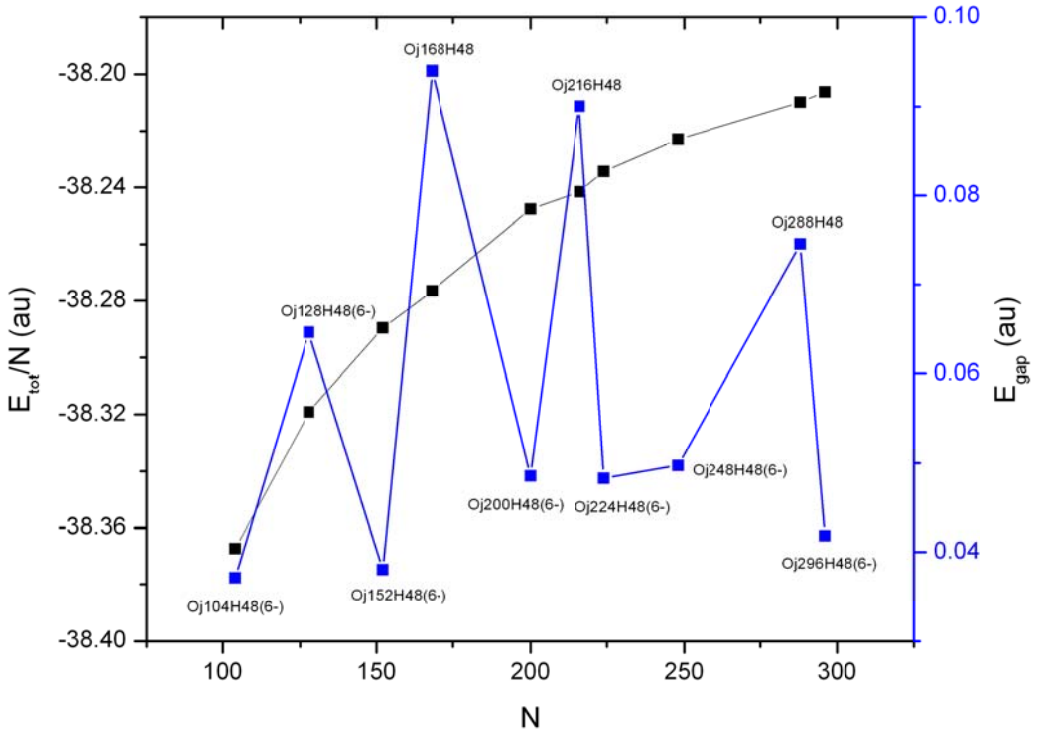

Figure 25 Plot of the octahedral junctions Oj(4,4) total energy per number of carbon atoms in a.u. and gap energy in a.u. as function of number of carbon atoms obtained from B3LYP/6-31G(d,p) single point energy calculations.

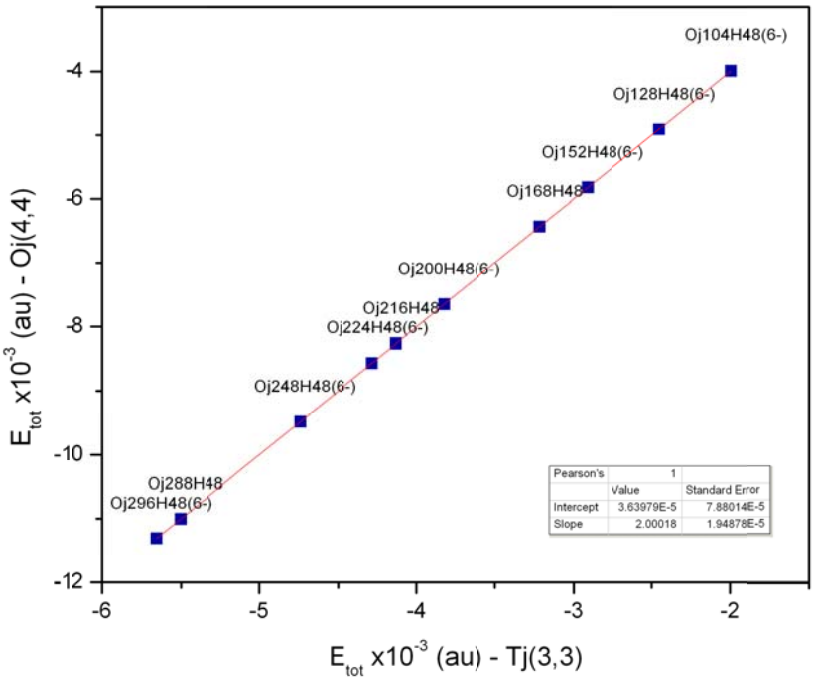

Figure 26 Plot of the total energy of octahedral junctions Oj(4,4) (E_{tot} in a.u.) as function of the total energy of the corresponding tetrahedral junctions Tj(3,3) (E_{tot} in a.u.) obtained from B3LYP/6-31G(d,p) single point energy calculations.

The plot of the total energy (a.u.) of the octahedral junctions Oj(4,4) as function of the total energy (a.u.) of tetrahedral junctions Tj(3,3) reflects that there is a strong linear relationship between the two set of structures (Figure 26). There is a perfect correlation between their energies (r value equals 1), and it must be noted that the slope equals almost 2, while the intercept is almost zero, meaning that the energy of the octahedral junction is twice the energy of the tetrahedral ones. This is in good agreement with the fact that the number of structural fragments is also twice in case of the octahedral junctions.

2.3. Tetrahedral junctions with attached nanotubes

To study the effect of the attached nanotube length on the stability of the junction [71], four series of tetrahedral junctions (3,3) with open ends were investigated by calculating the total energy and HOMO-LUMO gap energy for structures with different tube length.

The plot of the total energy per number of atoms (E_{tot}/N in kcal/mol) and gap energy (E_{gap} in a.u.) is presented in Figure 27 for the set of structures with the core junction Tj_{52}, Tj_{84}, Tj_{100} and Tj_{108}, respectively. In case of two series (Tj_{52} and Tj_{100}) neutral and charged structures were compared.

The results show that in all cases the gap energy decreases in an oscillating manner, while the total energy per number of atoms increases with the size of the nanotube. Thus the stability decrease is confirmed both kinetically and thermodynamically. Notice however that in the case of Tj_{52} junction set the total energy first slightly decreases within the series.

The neutral junctions have a much larger gap energy compared to the charged ones, also there is only a slight decrease along the series.

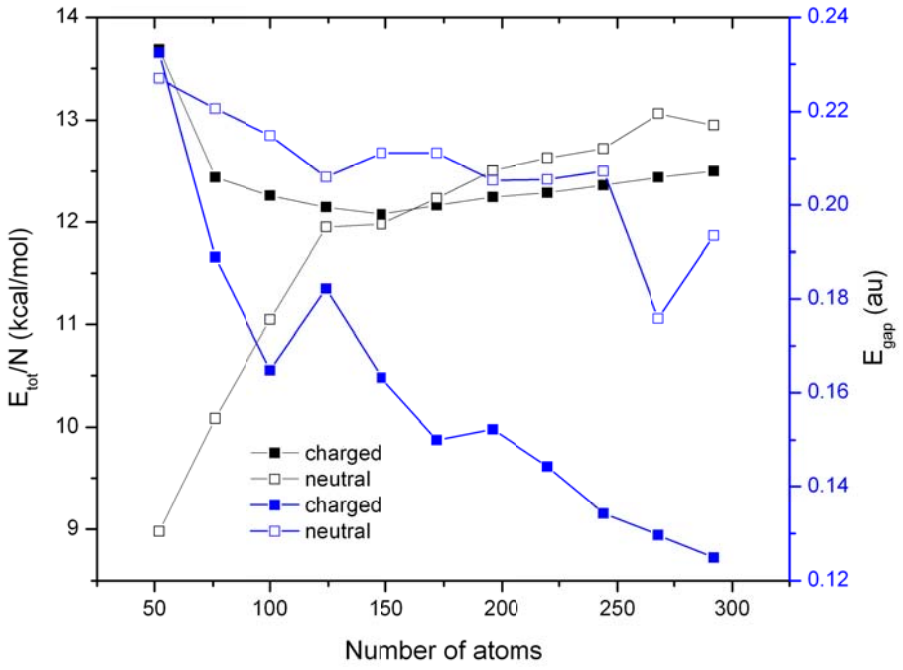

Figure 27 Plot of the total energy per number of atoms (E_{tot}/N in kcal/mol) and the gap energy (E_{gap} in a.u.) of the series of neutral and charged tetrahedral junctions Tj_{52} as function of the number of atoms, obtained from PM6 single point energy calculations.

2.4. Multiterminal junctions from C_{60} fullerene

Starting from the C_{60} fullerene set of junctions with one to four arms were built, where the length of the attached armchair nanotube was varied [71].

The total energy per atom (presented in Figure 32) increases with the nanotube length in all four series, however after a certain tube length the energy increment is very small. The stability increases with the number of the attached nanotubes (the number of terminals), thus the tetrahedral junctions are the most stable one.

Figure 33 presents the gap energy as function of the tube length, which in an oscillating manner decreases with the structure size, once again the most stable structures are the four-terminal junctions with the highest HOMO-LUMO gap values.

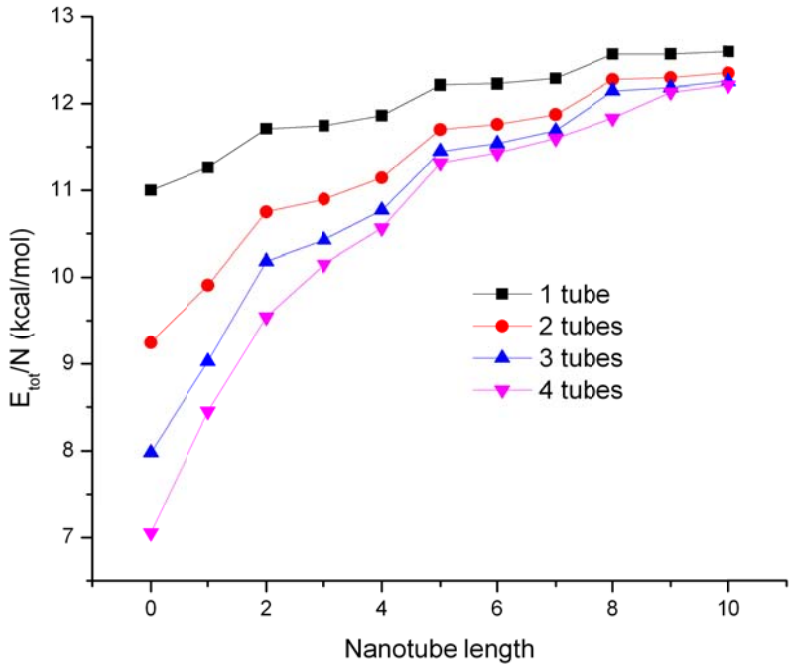

Figure 32 Plot of the total energy per number of atoms (E_{tot}/N in kcal/mol) of the series of junctions with one to four arms built from the C_{60}-I_h fullerene as function of the attached nanotube length, obtained from PM3 single point energy calculations.

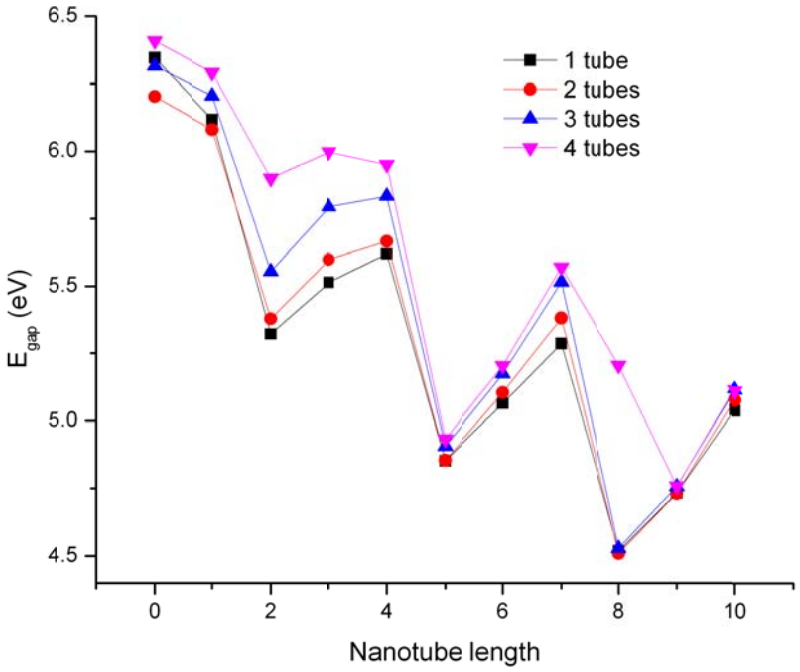

Figure 33 Plot of the gap energy (E_{gap} in eV) of the series of junctions with one to four arms built from the C_{60}-I_h fullerene as function of the attached nanotube length, obtained from PM3 single point energy calculations.

2.5. Conclusions

Tetrahedral fullerenes were generated and classified by the structural fragment and the correspondence with the derived tetrahedral junctions. A structurally corresponding series of octahedral junctions were built using structural fragments from the tetrahedral junctions. All molecules were optimized at the B3LYP/6-31G(d,p) level of theory. A linear correlation was found to exist between the total energies of the molecules. It was found that the energy per atom increases with the junction size. Kinetic stability favors the neutral junctions.

The increase in the length of the attached armchair (3,3) nanotube decreases the stability of the structure confirmed both kinetically and thermodynamically. The number of openings has a strong effect on the stability as compared within sets of multiterminal junctions. The stability increases with the number of terminals.

3.3. Computational study of armchair Yj(n,n) junctions

To study the effect of attached carbon nanotube on the stability of the Y junction, several series of structures were built where the length of the nanotube varies. Both opened, with hydrogenated openings, and closed (by nanotube caps) Y junctions were considered. For the closed structures two different nanotube caps was used. Only armchair symmetric junctions was studied, where the chirality of the opening is (4,4), (6,6) and (8,8), respectively. Each studied junction includes six heptagons, needed for the negative curvature where two tubes are joined, they are distributed in a symmetric way, each structure has D_{3h} symmetry.

In the case of Yj(6,6) nanotube junctions three different junction topologies was studied, which are different by the position of heptagons, and also by the number of carbon atoms. All heptagons are isolated, surrounded only by hexagons.

3.3.1. Opened symmetrical armchair Yj(n,n) junctions

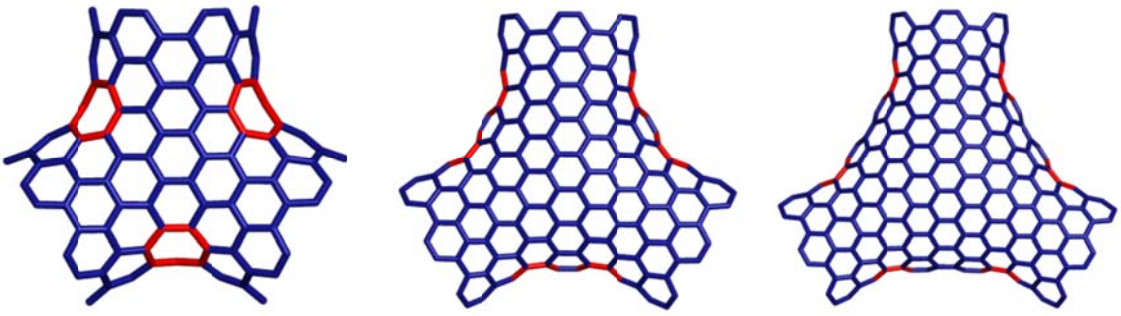

Yj(6,6)a - TU(6,6,3) Yj(6,6)b - TU(6,6,3) Yj(6,6)c - TU(6,6,3)

Figure 46 Three symmetric Y-type junctions with D_{3h} symmetry with (6,6) armchair openings, at each opening an armchair nanotube of length 3 is connected. The structures are viewed along the threefold axe C_3 (left), twofold axe C_2 top (center), and twofold axe C_2 bottom (right), respectively.

Yj(4,4)a - TU(4,4,2) Yj(8,8)a - TU(8,8,2)

Figure 47 Symmetric Y-type armchair junctions with D_{3h} symmetry Yj(4,4)a (top) and Yj(8,8)a (bottom), with chirality (4,4) and (8,8), respectively. To each junction an armchair nanotube of length 2 with matching chirality is attached, the structures are viewed along the threefold axe C_3 (left), twofold axe C_2 top (center), and twofold axeC_2 bottom (right).

In Figure 46 the symmetric armchair Y junctions are shown, with the opening chirality being (6,6) and an armchair nanotube of length 3 is attached. As it can be observed, the heptagons positions are different which gives the junction a different geometry. In the figures the optimized geometries are presented (hydrogen atoms are not shown), according to the junction geometry the shape of the attached nanotube changes, in one case it preserves its original circular shape, while in the other two cases the nanotube has an elliptic shape.

The Y junctions related to Yj(6,6)a are shown in Figure 47, they have (4,4) and (8,8) armchair chirality. Only in the case of Yj(6,6)a the attached nanotube preserves the circular shape, the other two junctions deforms it into an elliptical geometry.

The geometry optimization and single point energy calculations were performed at the PM6 semiempirical level of theory. As stability criterion two parameters were followed: the total energy divided by the number of carbon atoms, and the HOMO LUMO energy gap.

The results obtained for the series of Y junctions Yj(4,4)a, is presented in Figure 48, respectively. It can be observed that with the increment of the attached nanotube both the total energy and the gap energy oscillate with a periodicity of three. There is a good correlation between the kinetic and thermodynamic parameter, along the series both parameters sort order matches. In every case the gap energy decreases, however the total energy per atom in the case of Yj(4,4)a increases with the length of the tube. In the other two cases the tube length increases the stability of the structure.

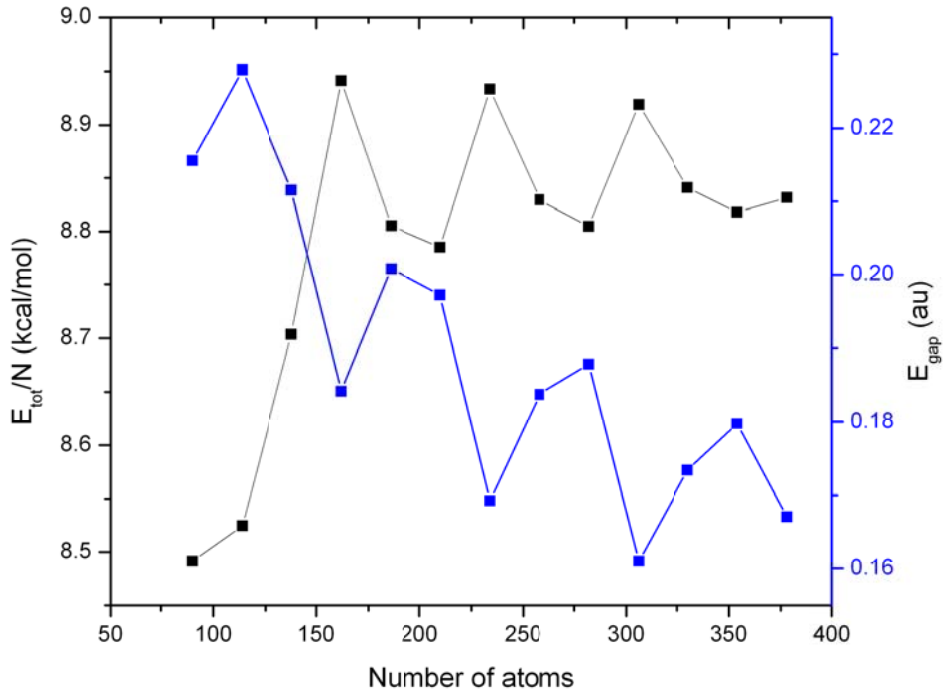

Figure 48 Plot of the total energy (kcal/mol) per number of carbon atoms (E_{tot}/N) and the HOMO-LUMO gap energy (E_{gap} in au) as function of the number of atoms, obtained with the PM6 semiempirical method for the series of opened Y-type junction Yj(4,4)a.

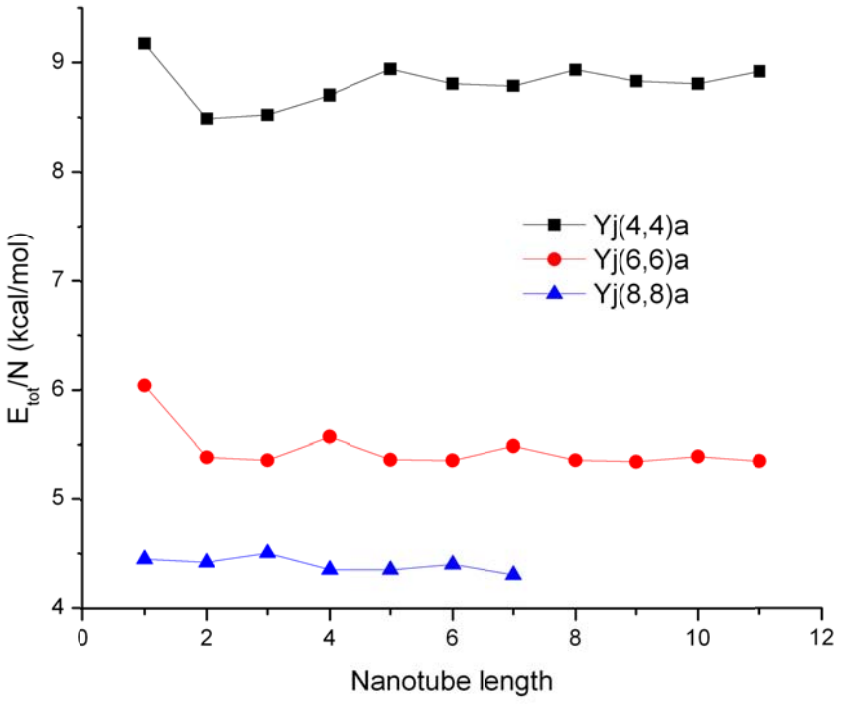

Figure 51 Plot of the total energy (kcal/mol) per number of carbon atoms (E_{tot}/N) as function of the attached nanotube length, obtained with the PM6 semiempirical method for the three series of opened Y-type junction Yj(4,4)a, Yj(6,6)a and Yj(8,8)a, respectively.

In Figure 51 the total energy per atom between the three series is compared. The highest values correspond to the Yj(4,4)a series, while the lowest on to the Yj(8,8)a junction series. It can be concluded that the nanotube diameter contributes to the stability of the junction, therefore the junction with the attached nanotube with largest diameter (8,8) is the most stable one.

This sort order however is not preserved when comparing gap values between the series as it can be seen in Figure 52. Notice however that the along one series the sort order cannot be related to the nanotube length. It can be observed that in each series the most stable structures correspond to a different nanotube length.

The periodic oscillation in the gap energy with the nanotube length was observed in case of opened or closed armchair nanotubes [31, 35-37, 97-103]. However no oscillation in the values of the total energy per atoms was observed.

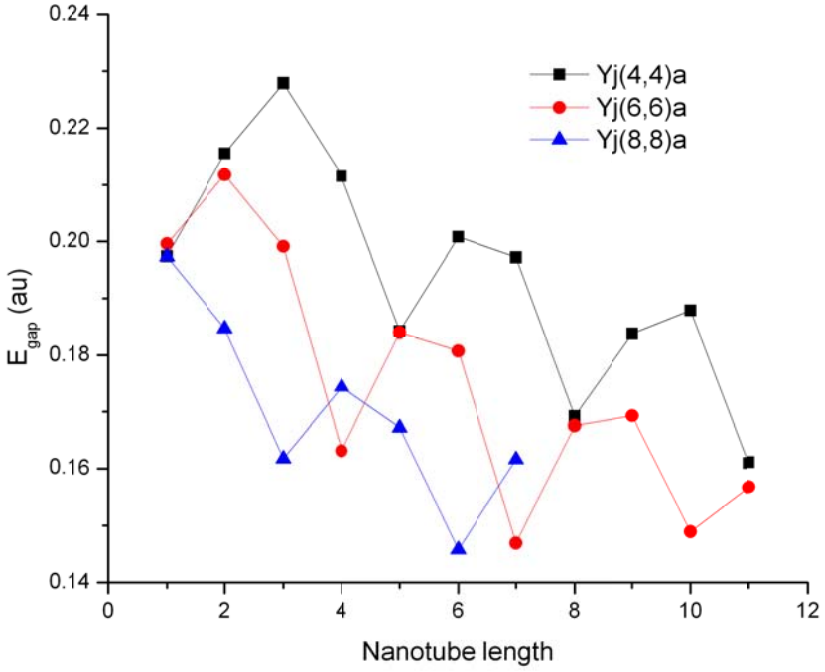

Figure 52 Plot of the HOMO-LUMO energy gap (E_{gap} in au) as function of the nanotube length, obtained at the PM6 semiempirical level of theory, for the three series of opened Y-type junctions: Yj(4,4)a, Yj(6,6)a and Yj(8,8)a, respectively.

The three opened armchair Yj(6,6) junctions stability is compared in Figure 53 (gap energy) and Figure 54 (total energy), respectively. The gap energy oscillation is almost identic along the three series, and the Yj(6,6)a has the highest gap values. This stability

ordering is contradicted by the next plot, however the total energy per atom values are very close at a given nanotube length. Notice that only in the case of Yj(6,6)a the total energy decreases with the tube length, at least in the structured considered in this study. It is possible that with a longer attached nanotube, the tube contributes more to the stability of the structure. The increase in energy can be attributed to the fact that the geometry of this short nanotube is distorted, and strain is introduced.

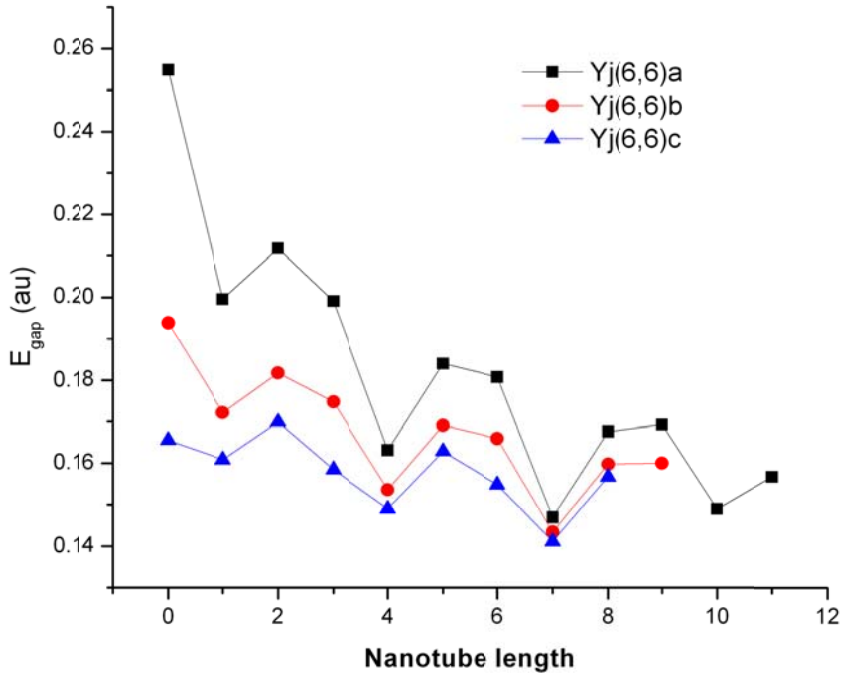

Figure 53 Plot of the HOMO-LUMO energy gap (E_{gap} in au) as function of the nanotube length, obtained at the PM6 semiempirical level of theory, for the three series of opened Y-type junctions: Yj(6,6)a, Yj(6,6)b and Yj(6,6)c, respectively.

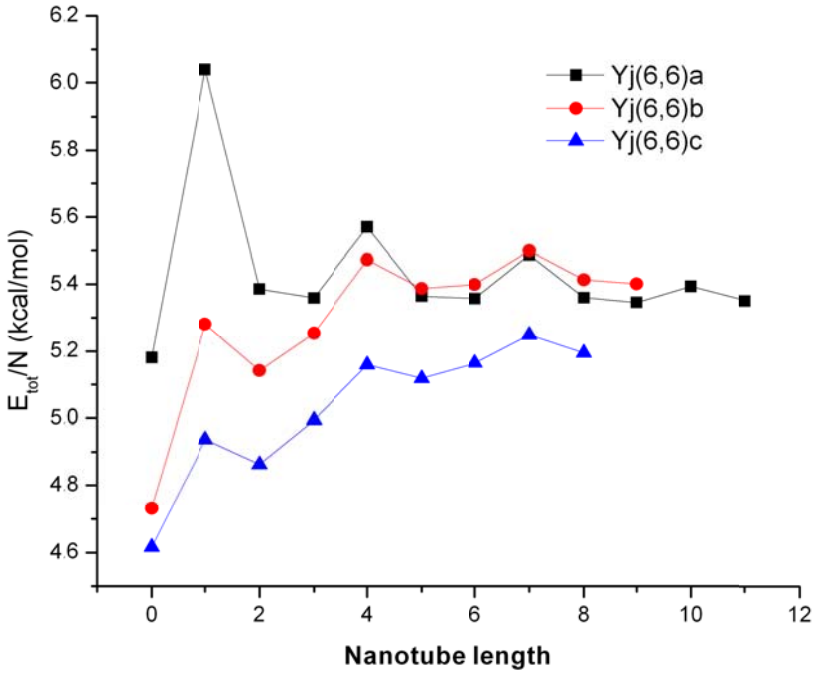

Figure 54 Plot of the total energy (kcal/mol) per number of carbon atoms (E_{tot}/N) as function of the attached nanotube length, obtained with the PM6 semiempirical method for the three series of opened Y-type junctions Yj(6,6)a, Yj(6,6)b and Yj(6,6)c, respectively.

3.3.2. Symmetric capped Yj(n,n) armchair junctions

To study the cap effect on the stability of the junction, the three armchair junction series Yj(6,6)a, Yj(6,6)b and Yj(6,6)c were closed a the opposing end of the nanotube with respect to the junction (Figure 57). The nanotube cap is a half fullerene, which includes 6 pentagons and has a positive curvature. One nanotube cap can fit to only on kind of nanotube, however a nanotube can be enclosed by more than one cap (depends on the size of the opening) [37, 104, 105]. To preserve the junction high symmetry only two symmetrical caps were chosen to close the structure, their structure viewed along the symmetry axe can be seen in Figure 58.

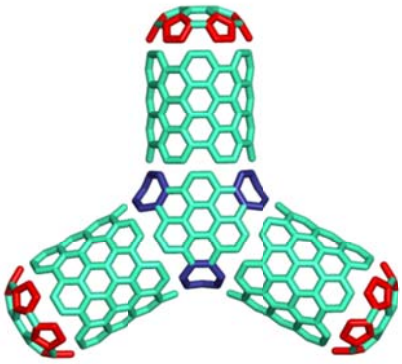

Figure 57 Construction of a closed Y-type junction Yj(6,6) from three fragments: the junction region (central) is characterized by negative curvature introduced by the heptagons, the three attached armchair nanotubes to the openings of the junction, and the nanotube caps that enclose the opposite send of the nanotube with respect to the junction, and which are characterized by the positive curvature introduced by the pentagons. The chirality of each structural element must be the same.

Figure 58 Armchair (6,6) carbon nanotube caps (half-fullerenes), with six-fold C_6 (left) – cap 1, and three-fold C_3 (right) –cap 2 rotational symmetry axe, respectively. Each cap contains 6 pentagons which gives a positive curvature to the structure.

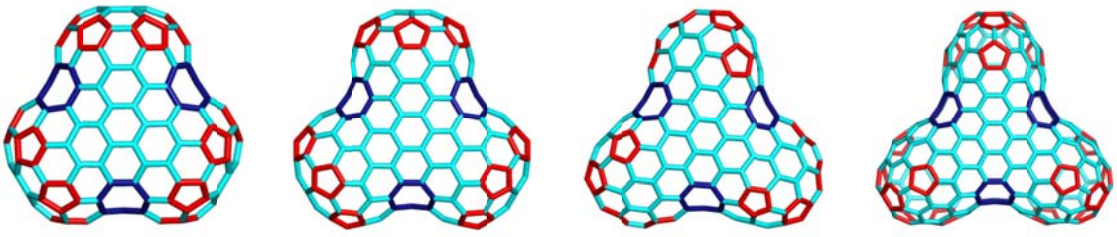

Yj(6,6)a cap1	Yj(6,6)a cap1	Yj(6,6)a cap2	Yj(6,6)a cap2
even number of rows	odd number of rows	even number of rows	odd number of rows

Figure 59 Y-type junction Yj(6,6)a closed at each end with the same nanotube cap. Depending on the attached nanotube length (odd or even) the cap changes its position relative to the junction.

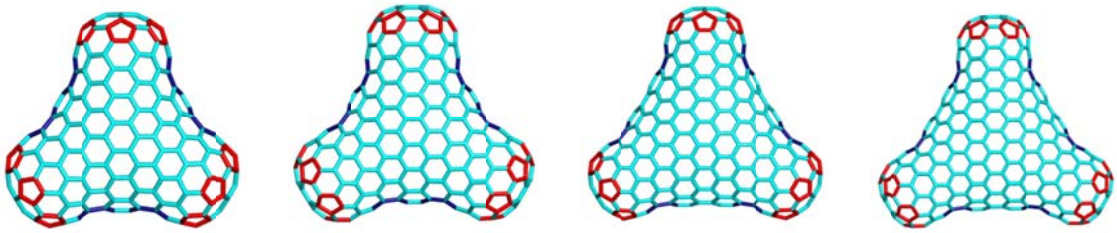

Yj(6,6)b1	Yj(6,6)b1	Yj(6,6)c1	Yj(6,6)c1
even number of rows	odd number of rows	even number of rows	odd number of rows

Figure 60 Closed symmetric Y junctions, Yj(6,6)b and Yj(6,6)c, capped at each opening using the same cap. The cap position varies depending on the length of the nanotube between the junction and cap (even and odd number of atom rows).

Series were constructed by increasing the length of the tube between the junction and the cap. Depending on the length of the nanotube (even or odd number of rows of atoms) the cap changes its position relative to the junction. Figure 59 presents the Yj(6,6)a capped with both nanotube caps, while Figure 60 shows the geometry of the Yj(6,6)b and Yj(6,6)c closed with cap 1.

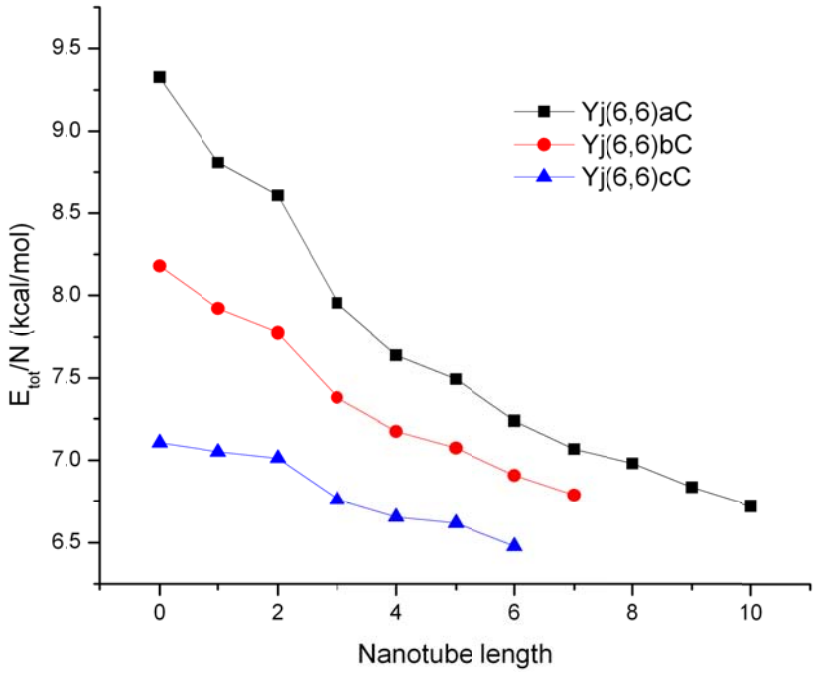

Figure 61 Plot of the total energy (kcal/mol) per number of carbon atoms (E_{tot}/N) as function of the length of the (6,6) armchair nanotube attached to the junction obtained with the PM6 semiempirical method for the series of closed Y-junctions: Yj(6,6)aC, Yj(6,6)bC, and Yj(6,6)cC.

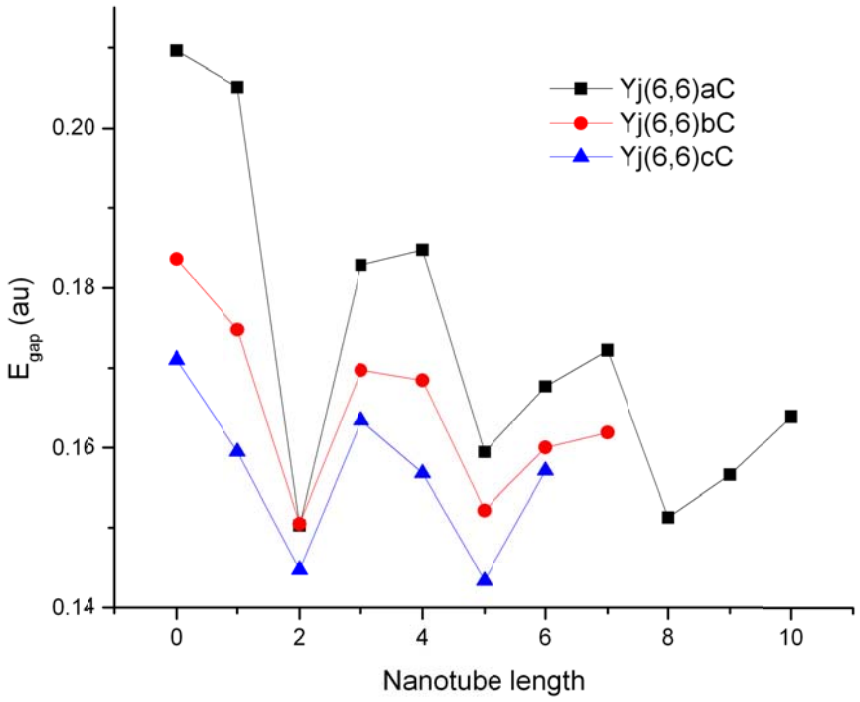

Figure 62 Plot of the HOMO-LUMO energy gap (E_{gap} in au) as function of the nanotube length, obtained at the PM6 semiempirical level of theory, for the three series of closed Y-type junctions: Yj(6,6)aC, Yj(6,6)bC și Yj(6,6)cC.

The plot of the total energy per atom as function of the nanotube length is presented in Figure 61. The stability ordering corresponds to that of the opened Y junctions. The only difference is that in all cases the total energy decreases with the increase of the attached nanotube.

As in the previous study the ordering of the three series changes in the case of the energy gap, as it can be seen in Figure 62. Once again the three curves are almost parallel, the structures with the largest gap corresponds to the Yj(6,6)a series.

In the Figure 64 the total energy per atom and the gap energy is plotted versus the nanotube length, respectively, in the case of the two series of closed Yj(6,6)a junctions capped with cap 1 and 2. It can be seen that although there is some minor energy difference, however they have almost the same stability. The periodicity in the gap values is present, the series closed with the higher symmetry cap is somewhat more stable.

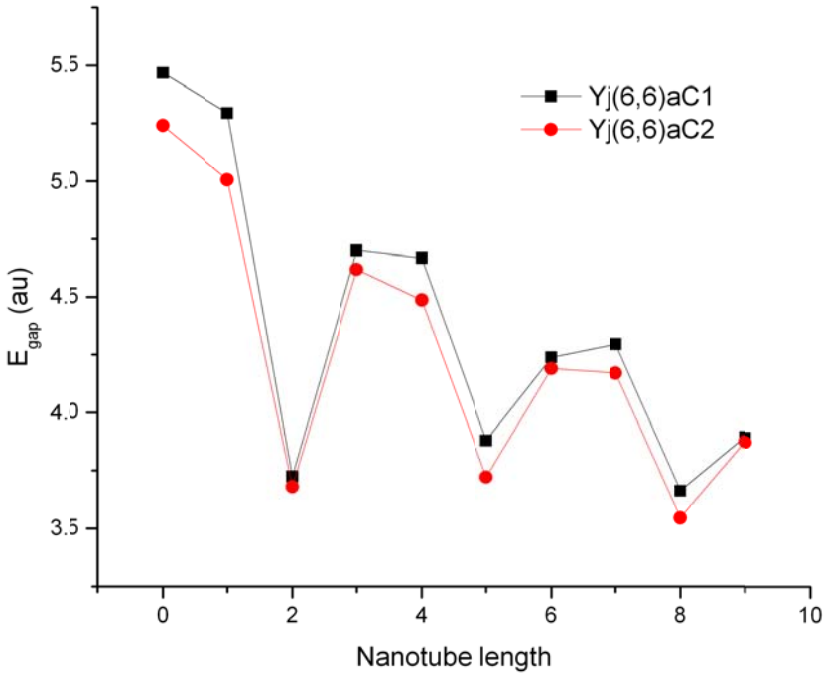

Figure 64 Plot of the HOMO-LUMO energy gap (E_{gap} in au) as function of the nanotube length, obtained at the PM3 semiempirical level of theory, for the two series of capped Y junctions: Yj(6,6)aC1 and Yj(6,6)aC2, respectively.

3.3.3. Closed asymmetric Yj(n,n) armchair junctions

Starting from the Yj(6,6)a junction four series of junctions were constructed by keeping constant two of the arms of the junctions, and increasing only one of the attached nanotube's length. Each nanotube was closed at the end with cap 1. An example is given in Figure 65 where two arms are of length 3, while the third nanotube is of length 8. The geometries were optimized with the PM3 semiempirical method.

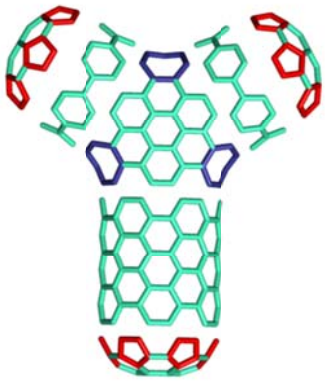

Figure 65 An example of asymmetric junction Yj(n,n): all attached nanotubes have the same chirality, but the length of one arm is different from the others.

Calculation results obtained at the same theoretical level are presented in Figure 66 and Figure 67, where the total energy per atom and the HOMO-LUMO gap energy are plotted as the function of the tube length, respectively. The first plot gives a similar answer as was previously observed in the case of closed Y junctions, which is the energy decreases with the tube length in all four series.

Notice however that in the second plot, not all series have the same stability ordering. Only the structures where the length of the tubes was zero and three, show a periodicity in the energy gap values. The two series stability is almost the same, with the exception of the first two members of the series. This could be explained by the fact, that every third member of these two series is a leapfrog structure [106-109].

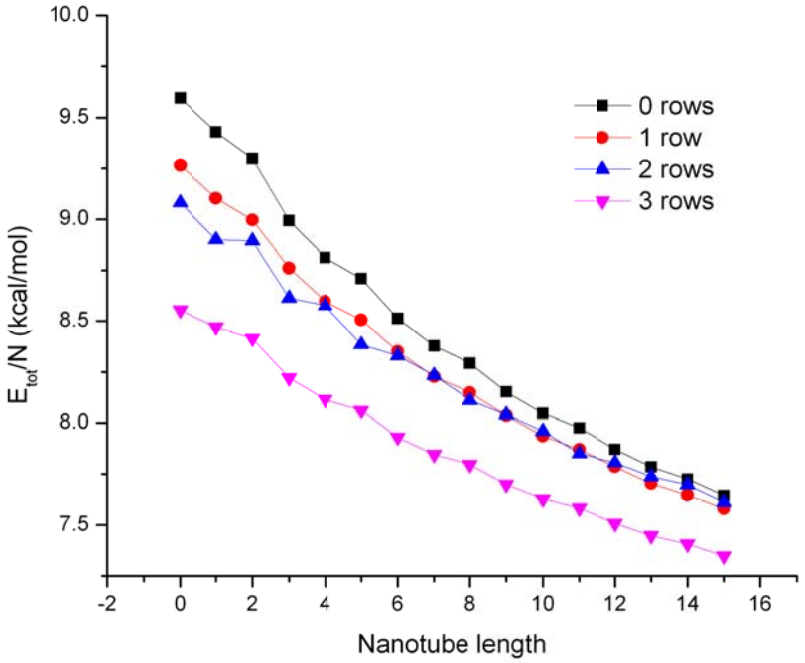

Figure 66 Plot of the total energy (kcal/mol) per number of carbon atoms (E_{tot}/N) as function of the attached (6,6) nanotube length, obtained with the PM3 semiempirical method for the four series of closed asymmetric Y-junctions.

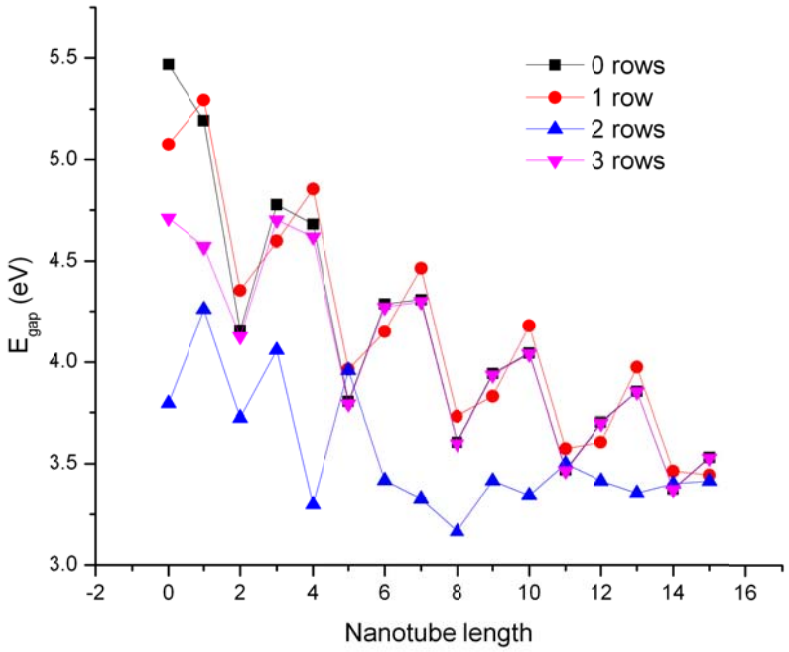

Figure 67 Plot of the HOMO-LUMO energy gap (E_{gap} in au) as function of the nanotube length, obtained at the PM3 semiempirical level of theory, for the four series of closed and asymmetric Y junctions.

3.4. Conclusions

To study the effect of the attached nanotubes on the stability of Y junctions, several series were modeled, where the nanotube length is increased. Also the opened junctions were closed by a nanotube cap, to study the cap effect. Geometry optimizations followed by single point energy calculations at the PM3 and PM6 semiempirical level of theory showed, that the nanotube length and diameter has a big influence on the stability. The closing cap didn't alter the stability sort order.

Similar to the armchair opened and closed nanotubes, an oscillating periodicity can be observed in the gap values of each series as function of the tube length. No direct relationship could be found between the stability and nanotube length, however the increase of the tube diameter decreases the total energy.

4.2. Topological description of nano dendrimers

Tetrapodal junctions were connected by identification (a procedure implemented in our software Nano Studio) to build dendritic molecules. Nano-dendrimers, at the first and second generation stages, respectively, are illustrated in Figure 68.

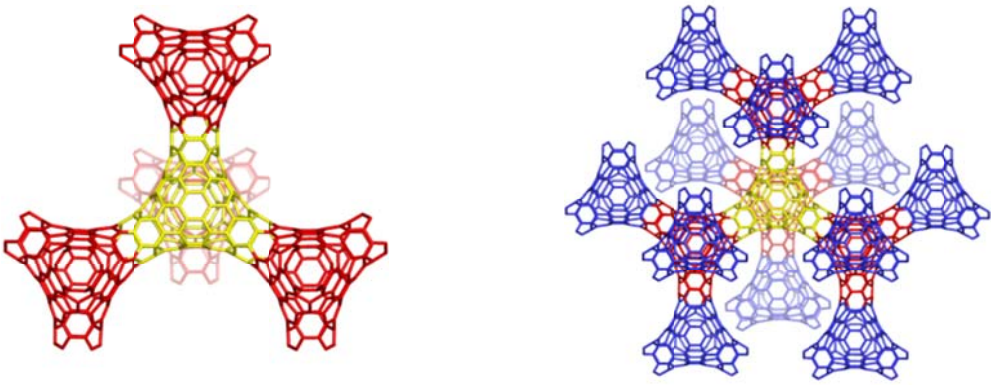

First dendrimer level Second dendrimer level

Figure 68 Dendrimer at first (left) and second (right) level built from C_{84} ($Le(Op(Le(Le(T))))$) tetrapodal junctions.

As above mentioned, a set of opposite or topologically parallel edges within the same face/ring eventually forming a strip of adjacent faces, is called a *qoc* or an *ops.* The number of *ops* of length *c* is given by the polynomial coefficients of terms at exponent *c*; the number of distinct c exponents equals the number of equivalence classes of opposite edges in G.

Analytical formulas of the Omega and Sadhana polynomial in tetrapodal junctions were derived [119]; in every formula, *m* represents the number of monomers. Examples of Omega, Sadhana polynomials and derived indices, in the case of dendrimers built up from tetrapodal junctions are presented in the tables below.

C_{84}-T_d-junction v =108 , f_6 = 28, f_7 = 12, e = 150

$Le_{11}(S_1(Le_{11}(Le_{11}(T))))$ TU3.3.0

Omega Polynomial $\Omega = 12(2m+1)X^1 + 24mX^3 + 6mX^7$

$\Omega'(G,1) = 138m + 12$

CI index $CI = 138^2 \cdot m^2 + 2778m + 132$; Example: $m = 3; CI = 179862$

Sadhana Polynomial $Sd = 12(2m+1)X^{138m+11} + 24mX^{138m+9} + 6mX^{138m+5}$

C_{84}-T_d-junction v = 132, f_6 = 40 f_7 = 12, e = 186

$Le_{11}(S_1(Le_{11}(Le_{11}(T))))$ TU3.3.1

Omega Polynomial $\Omega = 6(m+1)X^1 + 12(m+1)X^2 + (30m-6)X^3 + 6mX^9$

$\Omega'(G,1) = 174m + 12$

CI index $CI = 174^2 \cdot m^2 + 3366m + 144$; Example: $m = 5; CI = 773874$

Sadhana Polynomial $Sd = 6(m+1)X^{174m+11} + 12(m+1)X^{174m+10} + (30m-6)X^{174m+9} + 6mX^{174m+3}$

C_{60}-td-junction v = 84, f_6 = 16, f_7 = 12, e = 114

$Le_{11}(S_1(Ca_{21}(T)))$ TU3.3.0

Omega Polynomial $\Omega = 12(2m+1)X^1 + 12mX^2 + 18mX^3$

$\Omega'(G,1) = 102m + 12$

CI index $CI = 102^2 \cdot m^2 + 2214m + 132$; Example: $m = 2; CI = 46176$

Sadhana Polynomial $Sd = 12(2m+1)^{102m+11} + 12mX^{102m+10} + 18mX^{102m+9}$

C_{60}-td-junction v = 108, f_6 = 28 f_7 = 12, e = 150

$Le_{11}(S_1(Ca_{21}(T)))$ TU3.3.1

Omega Polynomial $\Omega = 6(m+1)X^1 + 12(m+1)X^2 + 6(6m-1)X^3$

$\Omega'(G,1) = 138m + 12$

CI index $CI = 138^2 \cdot m^2 + 2934m + 144$; Example $m = 4; CI = 316584$

Sadhana Polynomial $Sd = 6(m+1)X^{138m+11} + 12(m+1)X^{138m+10} + 6(6m-1)X^{138m+9}$

C_{120}-td-junction v = 144, f_6 = 46 f_7 = 12, e = 204

$Le_{11}(S_1(Le_{11}(Q_{2.0}(T))))$ TU3.3.0

Omega Polynomial $\Omega = 12(2m+1)X^1 + 12mX^3 + 6mX^4 + 12mX^6 + 3mX^{12}$

$\Omega'(G,1) = 192m + 12$

CI index $CI = 192^2 \cdot m^2 + 3516m + 132$; Example: $m = 2; CI = 154620$

Sadhana Polynomial $Sd = 12(2m+1)X^{192m+11} + 12mX^{192m+9} + 6mX^{192m+8} + 12mX^{192m+6} + 3mX^{192m}$

C_{120}-td-junction v = 168, f_6 = 58 f_7 = 12, e = 240

$Le_{11}(S_1(Le_{11}(Q_{2.0}(T))))$ TU3.3.1

Omega Polynomial $\Omega = 6(m+1)X^1 + 12(m+1)X^2 + 6(3m-1)X^3 + 18mX^6 + 3mX^{12}$

$\Omega'(G,1) = 228m + 12$

CI index $CI = 228^2 \cdot m^2 + 4176m + 144$; Example: $m = 7; CI = 2576592$

Sadhana Polynomial $Sd = 6(m+1)X^{228m+11} + 12(m+1)X^{228m+10} + 6(3m-1)X^{228m+9} + 18mX^{228m+6} + 3mX^{228m}$

C_{76}-td-junction TU3.3.0 v = 100, f_6 = 24 f_7 = 12, e = 138

Omega Polynomial $\Omega = 12(2m+1)X^1 + 12mX^2 + 6mX^3 + 12mX^5$

$\Omega'(G,1) = 126m + 12$

CI index $CI = 126^2 \cdot m^2 + 2598m + 132$; Example: $m = 2; CI = 68832$

Sadhana Polynomial $Sd = 12(2m+1)X^{126m+11} + 12mX^{126m+10} + 6mX^{126m+9} + 12mX^{126m+7}$

C_{76}-td-junction TU3.3.1 v = 124, f_6 = 36 f_7 = 12, e = 174

Omega Polynomial $\Omega = 6(m+1)X^1 + 12(2m+1)X^2 + 6(m-1)X^3 + 18mX^5$

$\Omega'(G,1) = 162m + 12$

CI index $CI = 162^2 \cdot m^2 + 3282m + 144$; Example: $m = 3; CI = 246186$

Sadhana Polynomial $Sd = 6(m+1)X^{162m+11} + 12(2m+1)X^{162m+10} + 6(m-1)X^{162m+9} + 18mX^{162m+7}$

The first derivative of Omega polynomial gives the number of the edges in *G*. The first derivative of Sadhana polynomials in x=1 is a multiple of the number of the edges, as shown above. The Cluj-Ilmenau CI index is a topological index, useful in correlating properties with molecular structures.

By construction, the "negative" polygon is 7 (an odd ring, with no opposite edges), so that the strip remains at the level of a single monomer unit and the polynomials are additive in their coefficients. In the above, "negative" refers to polygons inducing the negative curvature at the junction of tetrapodal units. The terms at *c*=1 (in Omega polynomial) account for the non-opposite edges or the odd rings.

Remark in these tables the simplicity at exponents of Omega *vs* Sadhana polynomials; the polynomial order increases as the size of fullerenes increases. The first derivative is 1st and 2nd order in *m*, for Omega and Sadhana, respectively. The value in x=1 is the same for both polynomials and accounts for the total number of strips. For the first three units, the same values $\Omega(G,1); Sd(G,1)$ are obtained, telling about their structural relatedness.

4.3. Topological description of networks built from P-type junctions

The studied P-type networks are periodic graphitic arrangements with hexagonal and heptagonal rings of carbon. They are a series of open networks made of sp^2 carbon atoms only. To the structures under study can connect six (4, 4) armchair carbon nanotubes, therefore a genus three. The topology of such P-type networks can be described by the aid of some counting polynomial, called Omega polynomial. Analytical formulas for counting polynomial, and derived indices, in P-type networks are given.

The unit cell of the Schwarz P (primitive) triply periodic minimal surface can be described as the intersection of six tubes coming through the faces of a cube, that meet into a 6–coordinated octahedral junction (also known as the "plumber's nightmare").

Two networks of 6-coordinated junctions were studied. The repeat units are obtained by a sequence of map operations starting from the cube, Le(Op(Le(Le(C)))) and

Le(Op(Le(Q(C)))) hereafter notated P216 and P288, respectively. Both the leapfrog Le and the chamfering Q transformations preserve the symmetry of the parent map, therefore the resulted junctions have the octahedral symmetry of the cube. By the introduction of one bivalent vertex on each edge of the 4-membered rings the structure is opened in six directions, indicating that it has genus 3. By the homeomorph transformation 24 hexagons became heptagons, which are all rotated in the final step (Le), resulting an opening with armchair (4,4) chirality.

In the P-type structures the number of ops of length c is given by the polynomial coefficients of terms at exponent c; the number of distinct c exponents equals the number of equivalence classes of opposite edges in G. Figure 71 illustrates qoc/ops.

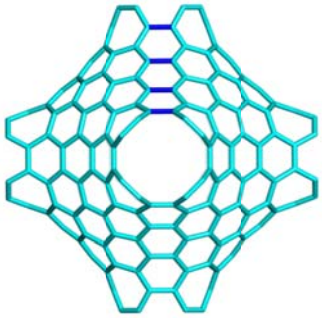

c = 4; *v* = 288; *e* = 408; f_6 =92; f_7=24

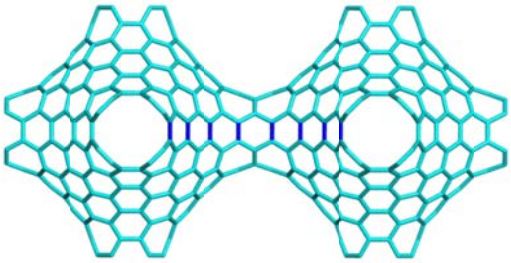

c = 8; *v* = 568; *e* = 812; f_6 = 188; f_7 = 48

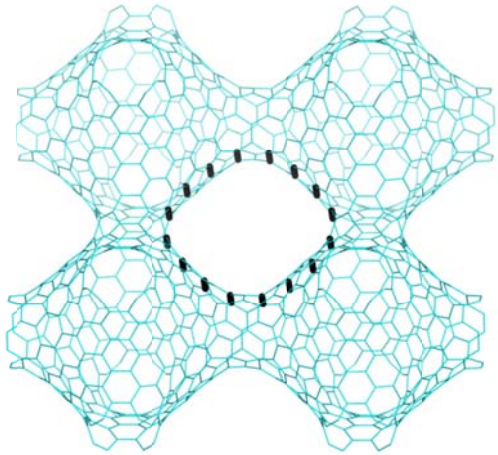

c = 16; *v* = 1120; *e* = 1616 ; f_6 = 384; f_7 = 96

Figure 71 Examples of Omega polynomial strips in case of $Le(Op(Le(Q(C))))$.

When two P-type junctions are connected the two *c* = 4 strips forms a continuous strip of length 8.When four junctions are connected in the shape of a square they will form a torus on the inside belt of the torus the two c = 8 strips will result a new strip of length 16. This strip is actually formed from the four c = 4 strips of the four junctions.

A complete network of P-type junctions can be defined in terms of three integers *a*, *b*, and *c*, their values represent the number of units along the three translation directions. Assigning numbers to these parameters is completely arbitrary and describes the same network (1×2×3 ≈ 2×1×3). A single unit is defined when all three integers are equal to one, denoted 1×1×1. Depending on the values of the parameters one can distinguish three cases of network types: *1*. the structure is linear if only one parameter is greater than one ($a > 1$, $b = c = 1$); *2*. the structure is two-dimensional if only one parameter equals one ($a, b > 1$, $c = 1$); *3*. when all the parameters have a value larger than one (a, b, $c > 1$), a three-dimensional structure is described.

An attempt to derive the Omega polynomial solely from the number of units (notated *u*) failed, because two distinct structures, although they have the same number of units (for example 1×1×8, 1×2×4 and 2×2×2 are all built from eight units), their polynomials are different. The case is similar when only the number of junctions (notated *j*) is taken into account.

The number of units (u), junctions (j), and tori (t) can be defined in terms of the structural parameters a, b, and c, the corresponding relationships are equations (8)-(12):

$$u = a \cdot b \cdot c \tag{44}$$

$$\begin{aligned} j &= (a-1)\cdot b \cdot c + a \cdot (b-1)\cdot c + a \cdot b \cdot (c-1) = \\ &= 3 \cdot a \cdot b \cdot c - (a \cdot b + b \cdot c + a \cdot c) = 3 \cdot u - (a \cdot b + b \cdot c + a \cdot c) \end{aligned} \tag{45}$$

$$(a \cdot b + b \cdot c + a \cdot c) = j - 3 \cdot u \tag{46}$$

$$\begin{aligned} t &= a \cdot (b-1)\cdot (c-1) + b \cdot (a-1)\cdot (c-1) + c \cdot (a-1)\cdot (b-1) = \\ &= 3 \cdot a \cdot b \cdot c - 2 \cdot (a \cdot b + b \cdot c + a \cdot c) + (a + b + c) = 4 \cdot j - 3 \cdot u + (a + b + c) \end{aligned} \tag{47}$$

$$(a + b + c) = t - 4 \cdot j + 3 \cdot u \tag{48}$$

Analytical formulas of Omega polynomial in case of $Le(Op(Le(Q(C))))$:

$$\Omega(X) = (72u - 20j)X^1 + 8jX^2 + 24uX^3 + 4(3u - 2j + t)X^4 + 24uX^6 + 4(j - t)X^8 + tX^{16} + 4uX^{18}$$

$$\Omega'(X) = 72u - 20j + 16jX + 72uX^2 + 16(3u - 2j + t)X^3 + 144uX^5 + 32(j - t)X^7 + 16tX^{15} + 72uX^{17}$$

$$\Omega'(1) = 408u - 4j$$

$$\Omega''(X) = 16j + 144uX + 48(3u - 2j + t)X^2 + 720uX^4 + 224(j - t)X^6 + 240tX^{14} + 1224uX^{16}$$

$$\Omega''(1) = 2232u + 144j + 64t$$

$$CI = (408u - 4j)^2 - 2640u - 140j - 64t$$

Analytical formulas of Omega polynomial in case of $Le(Op(Le(Le(C))))$:

$$\Omega(X) = (72u - 20j) \cdot X^1 + 8j \cdot X^2 + 48u \cdot X^3 + 4bc \cdot X^{7a} + 4ac \cdot X^{7b} + 4ab \cdot X^{7c}$$

$$\Omega'(X) = 72u - 20j + 16j \cdot X + 144u \cdot X^2 + 28abc\left(X^{7a-1} + X^{7b-1} + X^{7c-1}\right)$$

$$\Omega'(1) = 300u - 4j$$

$$\Omega''(X) = 16j + 288u \cdot X + 28abc\left((7a-1)X^{7a-2} + (7b-1)X^{7b-2} + (7c-1)X^{7c-2}\right)$$

$$\Omega''(1) = (196(a+b+c) + 204)u + 16j$$

$$CI = (300u - 4j)^2 - (196(a+b+c) + 504)u - 12j$$

4.4. Conclusions

Nano dendrimers built from two different tetrahedral junctions, and P-type networks built from octahedral junctions were characterized by means of Omega polynomial. Analytical formulas were derived in terms of repeat unit in case of dendrimers, and using three structural descriptors (number of units, junctions, tori) in case of the P-type networks.

References

1. HW Kroto, et al., *Nature* **318**(6042), 162-163 (1985).
2. W Kratschmer, et al., *Nature* **347**(6291), 354-358 (1990).
3. S Iijima, *Nature* **354**(6348), 56-58 (1991).
4. M Bockrath, et al., *Science* **275**(5308), 1922-1925 (1997).
5. YK Kwon, et al., *Physical Review Letters* **82**(7), 1470-1473 (1999).
6. SJ Tans, et al., *Nature* **393**(6680), 49-52 (1998).
7. BI Yakobson, et al., *American Scientist* **85**(4), 324-337 (1997).
8. H Terrones, et al., *Carbon* **30**(8), 1251-1260 (1992).
9. H Terrones, et al., *Chemical Physics Letters* **207**(1), 45-50 (1993).
10. D Ugarte, *Nature* **359**(6397), 707-709 (1992).
11. D Ugarte, *Chemical Physics Letters* **207**(4-6), 473-479 (1993).
12. AL Mackay, et al., *Nature* **352**, 762 (1991).
13. T Lenosky, et al., *Nature* **355**, 333-335 (1992).
14. M O'keeffe, et al., *Phys Rev Lett* **68**(15), 2325-2330 (1992).
15. H Terrones, et al., *Carbon* **30**(8), 1251-1260 (1992).
16. D Vanderbilt, et al., *Phys Rev Lett* **68**(4), 511-513 (1992).
17. JL Aragón, et al., *Phys Rev B* **48**(11), 8409-8413 (1993).
18. H Terrones, *J Math Chem* **15**, 143-156 (1994).
19. H Terrones, et al., *Acta Metall et Mater* **42**, 2687-2699 (1994).
20. H Terrones, et al., *J Math Chem* **15**, 183-195 (1994).
21. H Terrones, et al., *Chem Soc Rev* **24**, 341-350 (1995).
22. H Terrones, et al., *Prog Crystal Growth and Charact* **34**(1-4), 25-36 (1997).
23. RB King, *J Chem Inf Comput Sci* **38**, 180-188 (1998).
24. H Terrones, et al., *New Journal of Physics* **5**, 126.1-126.37 (2003).
25. F Valencia, et al., *New Journal of Physics* **5**, 123.1-123.16 (2003).
26. N Park, et al., *Phys Rev Lett* **91**(23), 237204(1-4) (2003).
27. JM Carlsson, et al., *Phys Rev Lett* **96**, 046806 (2006).
28. S Iijima, et al., *Journal of Chemical Physics* **104**(5), 2089-2092 (1996).
29. S Iijima, *Nature (London)* **354**, 56-58 (1991).
30. R Saito, et al., *Phys Rev B* **46**, 1804–1811 (1992).
31. A Rochefort, et al., *J Phys Chem B* **103**, 641-646 (1999).
32. W Liang, et al., *Journal of the American Chemical Society* **122**(45), 11129-11137 (2000).
33. N Park, et al., *Phys Rev B* **65**, 121405(1-4) (2002).
34. R Tamura, et al., *Phys Rev B* **52**, 6015–6026 (1995).
35. T Yumura, et al., *J Phys Chem B* **108**, 11426-11434 (2004).
36. S Reich, et al., *Phys Rev B* **72**, 165423(1-8) (2005).
37. SL Lair, et al., *Carbon* **44**, 447–455 (2006).
38. LA Chernozatonskii, *Physics Letters A* **170**(1), 37-40 (1992).
39. BI Dunlap, *Phys Rev B* **46**, 1933-1936 (1992).
40. J Han, *Chem Phys Lett* **282**, 187-191 (1998).
41. L Liu, et al., *Phys Rev B* **64**, 033412-1(4) (2001).
42. M Sano, et al., *Science* **293**(5533), 1299-1301 (2001).
43. M Huhtala, et al., *Comput Phys Commun* **147**(1-2), 91-96 (2002).
44. IG Cuesta, et al., *ChemPhysChem* **7**(12), 2503-2507 (2006).
45. K Sai Krishna, et al., *Chem Phys Lett* **433**(4-6), 327-330 (2007).
46. C Feng, et al., *Carbon* **47**(7), 1664-1669 (2009).

47. G Brinkmann, et al., *Match* **36**, 233-237 (1997).
48. G Brinkmann, et al., *Match* **63**(3), 533-552 (2010).
49. CL Nagy, et al., *Nano Studio*, 2010: Babes-Bolyai University.
50. JJP Stewart, *J Mol Model* **10**(2), 155-164 (2004).
51. JJP Stewart, *J Mol Model* **13**(12), 1173-1213 (2007).
52. J Tirado-Rives, et al., *J Chem Theory Comput* **4**(2), 297-306 (2008).
53. AD Becke, *Phys Rev A* **38**(6), 3098-3100 (1988).
54. C Lee, et al., *Phys Rev B* **37**(2), 785-789 (1988).
55. R Ditchfield, et al., *The Journal of Chemical Physics* **54**(2), 720-723 (1971).
56. PC Hariharan, et al., *Theor Chim Acta* **28**(3), 213-222 (1973).
57. MJ Frisch, et al., *Gaussian 09, Revision A.02*, 2009: Gaussian, Inc., Wallingford CT.
58. M Stefu, et al., *CageVersatile CVNet*, 2005: Babes-Bolyai University.
59. W Cheng, et al., *Journal of Molecular Structure: THEOCHEM* **489**(2-3), 159-164 (1999).
60. W Cheng, et al., *Journal of Molecular Spectroscopy* **193**(1), 1-6 (1999).
61. W Cheng, et al., *Journal of Electron Spectroscopy and Related Phenomena* **107**(3), 301-308 (2000).
62. AY Li, et al., *Physical Chemistry Chemical Physics* **2**(10), 2301-2307 (2000).
63. AC Tang, et al., *Chemical Physics Letters* **258**(5-6), 562-573 (1996).
64. AC Tang, et al., *Theoretical Chemistry Accounts* **102**(1-6), 72-77 (1999).
65. A Hirsch, et al., *Angewandte Chemie - International Edition* **39**(21), 3915-3917 (2000).
66. Z Chen, et al., *Journal of Molecular Modeling* **7**(5), 161-163 (2001).
67. Z Chen, et al., *Theoretical Chemistry Accounts* **106**(5), 352-363 (2001).
68. R Salcedo, et al., *Journal of Molecular Structure: THEOCHEM* **422**(1-3), 245-252 (1998).
69. M Lin, et al., *Journal of Molecular Structure: THEOCHEM* **489**(2-3), 109-117 (1999).
70. J Xiao, et al., *Journal of Molecular Structure: THEOCHEM* **428**(1-3), 149-154 (1998).
71. K Nagy, et al., *Fullerenes Nanotubes and Carbon Nanostructures* **18**(3), 216-223 (2010).
72. GE Scuseria, *Chemical Physics Letters* **195**(5-6), 534-536 (1992).
73. LA Chernozatonskii, *Physics Letters A* **172**(3), 173-176 (1992).
74. I Zsoldos, et al., *Modelling Simul Mater Sci Eng* **12**(6), 1251-1266 (2004).
75. I Zsoldos, et al., *Diamond Relat Mater* **14**, 763-765 (2005).
76. I Zsoldos, et al., *Modelling Simul Mater Sci Eng* **15**(7), 739-745 (2007).
77. GK Dimitrakakis, et al., *Nano Lett* **8**(10), 3166-3170 (2008).
78. E Tylianakis, et al., *Chem Commun (Cambridge, U K)* **47**(8), 2303-2305 (2011).
79. I László, *Croatica Chemica Acta* **78**(2), 217-221 (2005).
80. I László, *Fullerenes Nanotubes and Carbon Nanostructures* **13**(SUPPL. 1), 535-541 (2005).
81. I László, *Croatica Chemica Acta* **81**(2), 267-272 (2008).
82. I Ponomareva, et al., *New Journal of Physics* **5**, 119.1–119.12 (2003).
83. LP Biró, et al., *Diamond and Related Materials* **11**(3-6), 1081-1085 (2002).
84. LP Biró, et al., *Materials Science and Engineering C* **19**(1-2), 3-7 (2002).
85. LP Biró, et al., *Diamond and Related Materials* **13**(2), 241-249 (2004).
86. D Zhou, et al., *Chemical Physics Letters* **238**(4-6), 286-289 (1995).
87. GI Márk, et al., *Physical Review B* **58**(19), 12645-12648 (1998).
88. BC Satishkumar, et al., *Applied Physics Letters* **77**(16), 2530-2532 (2000).
89. WZ Li, et al., *Applied Physics Letters* **79**(12), 1879-1881 (2001).
90. J Li, et al., *Nature* **402**(6759), 253-254 (1999).
91. YC Sui, et al., *Journal of Physical Chemistry B* **105**(8), 1523-1527 (2001).
92. YC Sui, et al., *Carbon* **39**(11), 1709-1715 (2001).
93. AA Koós, et al., *Materials Science and Engineering C* **23**(1-2), 275-278 (2003).
94. M Terrones, et al., *Physical Review Letters* **89**(7), 075505/1-075505/4 (2002).
95. M Terrones, et al., *Microscopy and Microanalysis* **9**(SUPPL. 2), 320-321 (2003).
96. M Terrones, et al., *New Diamond and Frontier Carbon Technology* **12**(5), 315-323 (2002).
97. L Stobinski, et al., *Reviews on Advanced Materials Science* **5**(4), 363-370 (2003).

98. J Cioslowski, et al., *Journal of the American Chemical Society* **124**(28), 8485-8489 (2002).
99. T Yumura, et al., *Journal of the American Chemical Society* **127**(33), 11769-11776 (2005).
100. T Sato, et al., *Synthetic Metals* **103**, 2525-2526 (1999).
101. T Yaguchi, et al., *Physica B* **323**, 209-210 (2002).
102. Y Matsuo, et al., *Organic Letters* **5**(18), 3181-3184 (2003).
103. T Yumura, et al., *Chemical Physics Letters* **386**, 38-43 (2004).
104. G Brinkmann, et al., *Chemical Physics Letters* **315**(5-6), 335–347 (1999).
105. G Brinkmann, et al., *Discrete Applied Mathematics* **116**, 55–71 (2002).
106. PW Fowler, et al., *J CHEM SOC, CHEM COMMUN*, 1403-1405 (1987).
107. PW Fowler, *J CHEM SOC FARADAY TRANS* **86**(12), 2073-2077 (1990).
108. P Fowler, et al., *J CHEM SOC FARADAY TRANS* **90**(19), 2865-2871 (1994).
109. KM Rogers, et al., *J Chem Soc, Perkin Trans* **2**, 18–22 (2001).
110. MV Diudea, *Carpathian Journal of Mathematics* **22**(1-2), 43-47 (2006).
111. MV Diudea, et al., *Journal of Mathematical Chemistry* **45**(2), 316-329 (2009).
112. DZ Djokovic, *J Combin Theory Ser B* **14**, 263-267 (1973).
113. PM Winkler, *Discr Appl Math* **8**, 209-212 (1984).
114. MV Diudea, et al., *Croatica Chemica Acta* **79**(3), 445-448 (2006).
115. MV Diudea, et al., *Acta Chimica Slovenica* **57**(3), 565-570 (2010).
116. MV Diudea, et al., *Carpathian Journal of Mathematics* **25**(2), 177-185 (2009).
117. MV Diudea, et al., *Match* **60**(1), 237-250 (2008).
118. F Gholami-Nezhaad, et al., *Studia Universitatis Babes-Bolyai Chemia* (4), 219-224 (2010).
119. MV Diudea, et al., *Match* **65**(1), 143-152 (2011).
120. MV Diudea, et al., *Carpathian Journal of Mathematics* **26**(1), 59-66 (2010).
121. MV Diudea, *Journal of Mathematical Chemistry* **45**(2), 309-315 (2009).
122. MV Diudea, et al., *Match* **60**(3), 945-953 (2008).
123. M Saheli, et al., *Studia Universitatis Babes-Bolyai Chemia* **1**, 83-90 (2010).
124. MV Diudea, *Match* **63**(1), 247-256 (2010).
125. K Nagy, et al., *Studia Universitatis Babes-Bolyai Chemia* **1**, 77-82 (2010).
126. AE Vizitiu, et al., *Match* **60**(3), 927-933 (2008).
127. A Ilić, et al., *Carpathian Journal of Mathematics* **26**(2), 193-201 (2010).
128. MV Diudea, et al., *Studia Universitatis Babes-Bolyai Chemia* **4**(2), 313-320 (2009).
129. MV Diudea, et al., *Match* **65**(1), 131-142 (2011).

Scientific communications

1. MolMod 2007, Molecular modeling in chemistry and biochemistry, July, 5-8, Arcalia
   Diamond and dodecahedron architectures from carbon tetrapods (poster)
2. ChemMod 2007, Chemical Graph Theory and Molecular Modeling Workshop, October, 23-26, Cluj-Napoca
   Armchair [3,3] carbon nanotube junctions with tetrahedral symmetry (poster)
3. MolMod 2009, Molecular modeling in chemistry and biochemistry, April, 2-4, Cluj-Napoca
   Omega polynomials of carbon tetrapodal graphitic junctions (poster)
4. ICAM 2010 - "Mathematical Chemistry in NANO-ERA" Minisymposium, September, 1-4, Cluj-Napoca
   Y junctions from armchair carbon nanotubes(lecture)

Articles

1. Katalin Nagy, Csaba L Nagy, Gabriel Katona, Mircea V. Diudea
   Armchair [3,3] carbon nanotube junctions with tetrahedral symmetry
   Fullerenes, Nanotubes and Carbon Nanostructures, 18 (2010) 216-223
2. Katalin Nagy, Csaba L Nagy, Mircea V. Diudea,
   Omega polynomial in diamond-like dendrimers,
   Studia Univ. "*Babes-Bolyai*" *Chemia*, 55 (2010) 77-82
3. Mahboubeh Saheli, Mahdieh Neamati, Katalin Nagy, Mircea V. Diudea
   Omega polynomial in Sucor network,
   Studia Univ. "*Babes-Bolyai*" *Chemia*, 55 (2010) 83-90
4. Mahsa Ghazi, Modjtaba Ghorbani, Katalin Nagy, Mircea V. Diudea
   On Omega Polynomial of ((4,7)3) Network
   Studia Univ. "Babes-Bolyai" Chemia, 4 (2010) 197-200
5. Katalin Nagy, Csaba L Nagy, Mircea V. Diudea
   Omega and Sadhana polynomials of dendrimers designed from tetrapodal graphitic junctions
   MATCH Commun. Math. Comput. Chem, 65 (2011) 163-172
6. Mircea V. Diudea, Katalin Nagy, Csaba L Nagy, Aleksandar Ilić
   Omega polynomial in puzzle zeolites
   MATCH Commun. Math. Comput. Chem, 65 (2011) 143-152